RESEARCH PAPER

Suction-enhanced siphon valves for centrifugal microfluidic platforms

**Robert Gorkin · Salar Soroori · William Southard ·
Liviu Clime · Teodor Veres · Horacio Kido ·
Lawrence Kulinsky · Marc Madou**

Abstract In traditional centrifugal microfluidic platforms pumping is restricted to outward fluid flow, resulting in potential real estate issues for embedding complex microsystems. To overcome the limitation, researchers utilize hydrophilic channels to force liquids short distances back toward the disk center. However, most polymers used for CD fabrication are natively hydrophobic, and creating hydrophilic conditions requires surface treatments/specialized materials that pose unique challenges to manufacturing and use. This work describes a novel technology that enjoys the advantages of hydrophilic fluidics on a hydrophobic disk device constructed from untreated polycarbonate plastic. The method, termed suction-enhanced siphoning, is based on exploiting the non-linear hydrostatic pressure profile and related pressure drop created along the length of a rotating microchannel. Theoretical analysis as well as experimental validation of the system is provided. In addition, we demonstrate the use of the hydrostatic pressure pump as a new method for priming hydrophobic-based siphon structures. The development of such techniques for hydrophobic fluidics advances the capabilities of the centrifugal microfluidic platform while remaining true to the goal of creating disposable polymer devices using feasible manufacturing schemes.

Robert Gorkin, Salar Soroozi and Liviu Clime contributed equally to this work.

R. Gorkin (✉) · S. Soroori · W. Southard · M. Madou
Department of Biomedical Engineering,
University of California, Irvine, Irvine, CA 92697, USA
e-mail: rgorkin@uci.edu

L. Clime · T. Veres
National Research Council—Industrial Materials Institute,
Boucherville, QC J4B 6Y4, Canada

H. Kido · L. Kulinsky · M. Madou
Department of Mechanical & Aerospace Engineering,
University of California, Irvine, Irvine, CA 92697, USA

H. Kido
RotaPrep, Inc., Tustin, CA 92782, USA

M. Madou
UNIST, World Class University (WCU), Ulsan, South Korea

1 Introduction

Centrifugal pumping forms the basis of propulsion in CD-based microfluidic platforms; spinning a disk induces pressure on fluids held inside chambers/channels and drives samples outward from the center of the disk (Ducrée et al. 2007; Madou et al. 2006). As a direct result of the unidirectional flow, fluidic conduits in such devices must conform to an "outwardly" orientation such that liquids can be forced from centrally located chambers to more peripheral ones. The alignment is a considerable limitation for centrifugal platforms since it confines the space for the number of microfluidic processes and thus the complexity of an assay performed on the disk. Simple systems involving only a few liquid manipulation steps, such as in the automated mixing of reagents in clinical chemistry (Burtis et al. 1972), might not require more sophisticated designs, but limited CD real estate can bring serious challenges to more

integrated assays demanding multiple sequential sample handling operations (e.g., preparation and detection of pathogens from clinical samples (Gorkin et al. 2010a)). By addressing the shortcomings of restricted area in CD-based platforms, more advanced analysis with complex integrated processing could become possible.

To overcome spaces issues, researchers have tackled how multiple reagents are stored, held, and transferred "on-command" during processing, mainly through augmented centrifugal pumping and valving techniques. A common technique uses the interplay between capillary forces and centrifugal forces to direct fluid movement. In general, the direction of the action of surface tension forces depends on the contact angle that fluid makes with the surface of the microchannel, and many polymers from which centrifugal platforms are made of are natively hydrophobic (Tsao and DeVoe 2009; Becker and Gärtner 2008). In such systems, we term "hydrophobic fluidics", the surface tension forces will oppose the movement of the fluid through microchannels and will act against centrifugal forces on a disk. Alternatively, through the use of special treatments (Siegrist et al. 2010) or with specific materials (García-Cordero et al. 2010b), surfaces in centrifugal systems can be rendered hydrophilic. In such "hydrophilic fluidics", surface tension forces push the fluid through the channels and centrifugal force can act either with (if fluid wetting direction is toward the edge of the disk) or against capillary forces (when capillary meniscus advances from the edge of the disk toward the center of the disk).

In terms of centrifugal microfluidic technology, hydrophilic fluidics has been used to counter centrifugally driven flow; fluids are first centrifuged outwardly at high angular velocities, and then, a reduction in spin speed allows capillary forces to pump liquids in the opposite direction (toward the central point in a CD) when the capillary force overcomes the centrifugal force. The principle has often been adapted for siphoning on a disk (for example in Siegrist et al. 2010; Steigert et al. 2007; Kido et al. 2007) as capillary forces allow for siphon priming at low enough angular velocities, where capillary force dominates and moves the fluid through wetting the siphon microchannel. Passive fluid flow driven by capillary force toward the center of a disk can be advantageous for the purpose of maximizing the use of real estate available on the disks and processing of complex assays. However, as alluded to previously, plastics that are used in disk fabrication are in general hydrophobic and typically require additional treatments to make them more hydrophilic. Often though, the contact angle on modified plastic surfaces has poor long-term stability (Beaulieu et al. 2009; Larsson and Derand 2002). This presents a problem since fluidic behavior alters as contact angle of surface-modified

plastics changes over time. An additional consideration is higher manufacturing cost for hydrophilic platforms due to the additional treatment(s) they require.

The work herein describes a new technology that recreates the advantages of hydrophilic fluidics for siphon valving in a hydrophobic CD platform. The technique, termed "suction-enhanced siphoning", exploits the localized pressure differences created along the length of a microchannel during natural fluid movement using centrifugal pumping. We first outline the concept of the proposed suction-enhanced siphoning technique followed by the analytical description of the system that includes the design criteria for fabricating such pumps. Results from the experiments are then used to validate the analytical model. Following the analytical section, a valving concept is presented using the hydrostatic pressure pumping for priming a siphon under hydrophobic conditions on the centrifugal platforms. Finally, use of hydrostatic pressure pumps in disk-based systems is discussed for general utility toward more complex assays on lab-on-a-CD platforms.

2 Concept

The proposed technique for pumping liquids and related suction-enhanced siphon valves are based on a phenomenon that occurs during centrifugal fluid transfer in a straight radial microchannel on a rotating disk. During rotation, for steady and continuous fluid flow, there is a non-uniform distribution of centrifugal forces in the microchannel. The related non-linear pressure profile is caused by the non-uniformity of centrifugal forces within the microsystem and the transient nature of the hydrostatic pressure in the loading reservoir (Fig. 1). The analytical model (discussed in Sect. 3) describes the resulting parabolic pressure profile along the microchannel. The pressure at the outlet equals the atmospheric pressure, while at the inlet the pressure is higher due to hydrostatic pressure generated by the liquid in the loading reservoir. The basic principle of the proposed pumping technique relies on the regions of pressure drop in the rotating radial channel to create suction in an adjacent channel (that could be connected to a fluid reservoir and/or a siphon valve). As shown in Fig. 1, an auxiliary microchannel joins a main radial fluidic conduit forming a T-junction. During operation on a rotating disk, fluid from the radial channel first enters into the secondary channel (during the backfilling stage of the process) and then moves in the opposite direction (when sufficient negative pressure is created in the radial channel). This operation can be described as a pressure switch, which can be used to pump fluid. If the design incorporates an additional reservoir connecting to the auxiliary microchannel,

Fig. 1 Schematic showing the influence of the hydrostatic pressure head throughout the microchannel in a centrifugal platform. **a** Profile view of the centrifugal microfluidic structure; **b–e** pressure profile changes in the microchannel during emptying
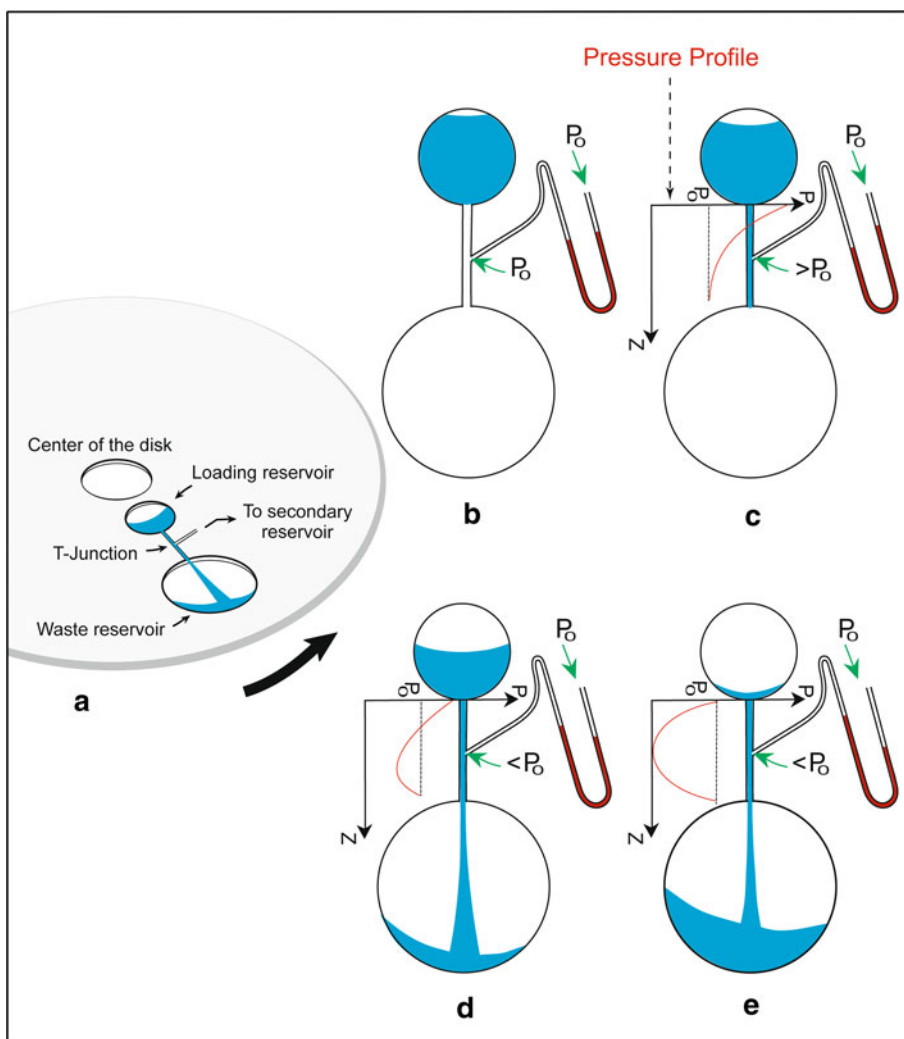
that pressure switch will create a suction effect that triggers fluid flow from the auxiliary reservoir into the main radial microchannel. Under certain conditions, defined below, this technique can be used as a hydrophobic siphon valve, where the suction effect can efficiently siphon fluids from isolated chambers on a disk.

3 Analytical model

In the following section, we describe the dynamic pressure generation that occurs along a microchannel during disk rotation. The steady state flow of an incompressible Newtonian fluid (e.g., water) is described by the time-independent form of the Navier–Stokes equations:

$$0 = -\nabla p + \mu \nabla^2 \vec{v} + \vec{f} \tag{1}$$

Here, p stands for the static pressure, μ the dynamic viscosity, $\vec{v}$ the fluid velocity, and $\vec{f}$ a term representing the body forces. For a rectangular channel of width $2a$ and

height $2b$, the behavior of the fluid can be obtained by solving the above Navier–Stokes equations for v_z, the longitudinal component of the velocity (radial direction), and the solution reads:

$$v_z(x,y) = \frac{16}{\pi^2 \eta}\left(-\frac{dp}{dz}+f\right)\sum_{m=1}^{\infty}\sum_{n=1}^{\infty}\frac{(-1)^{m+n}}{(2m-1)(2n-1)\lambda_{m,n}}$$
$$\times \cos\frac{\beta_m x}{a}\cos\frac{\beta_n y}{b} \tag{2}$$

where

$$\lambda_{m,n} = \frac{\beta_m^2}{a^2}+\frac{\beta_n^2}{b^2}$$

$$\beta_m = \pi\left(m-\frac{1}{2}\right)$$

$$\beta_n = \pi\left(n-\frac{1}{2}\right)$$

All the terms in Eq. 2 (derived in Liu et al. 2008) are z-independent except for the term in the parenthesis

$-\frac{dp}{dz} + f$. Based on continuity equation for a channel with constant cross-sectional area, the fluid velocity along the z-axis is constant. Hence, the term $-\frac{dp}{dz} + f$ is constant, that is:

$$\frac{-dp}{dz} + f = C \tag{3}$$

This condition is the key to understanding the physics of the hydrostatic pressure pump. Since C is proportional to the fluid velocity, this equation can also be regarded as a differential form of the Bernoulli equation. In this view, f is responsible for the position-dependent pressure term.

We now consider a microchannel, connected to a large loading reservoir R (Fig. 2a) at one end and a waste reservoir
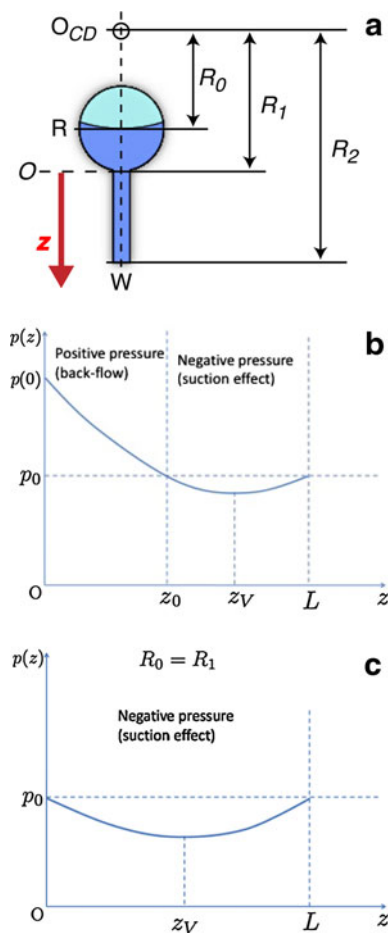

Fig. 2 a Schematics outlining a section of a straight microfluidic channel connected to the reservoir R and the waste chamber W; **b** pressure distribution along the radial microchannel on a disk rotating with a constant angular frequency. The terms "positive" and "negative" pressure refer to the difference with respect to the normal atmospheric pressure (so-called gauge pressure); **c** distribution of the static pressure along the channel from the inlet (z_0) to outlet (L) immediately after the emptying of the reservoir ($R_0 = R_1$). Pressure distribution has a shape of a symmetric parabola with the minimum value in the middle of the channel

(denoted W) at the other end. By "large loading reservoir," we mean that its volume is large enough to result in negligibly small fluid velocity emptying the reservoir as compared to the fluid velocity in the microchannel. Both chambers are connected to air vents in order to maintain atmospheric pressure, p_0. Center of rotation is point O_{CD} in the plane of Fig. 2a and ω is the angular frequency. We also define the following quantities: R_0 is the distance from O_{CD} to the top level of the liquid in the reservoir R, R_1 the distance from O_{CD} to the upper end of the channel and R_2 the distance from O_{CD} to the lower end of the channel.

We proceed to find the static pressure distribution $p(z)$ along the radial microchannel when the system in Fig. 2a is spinning at an angular frequency ω. The body force f in the equations above is z-dependent and originates from the centrifugal force due to rotation:

$$f = \rho\omega^2 r = \rho\omega^2(z + R_1) \tag{4}$$

where ρ is the fluid density and r is the distance of the fluid element from O_{CD} (center of rotation).

By integrating Eq. 3 from $z = -(R_1 - R_0)$ to $z = 0$ using Eq. 4 and taking into account that $C = 0$ in this interval (fluid velocity in reservoir R is nearly zero compared to the fluid velocity in the microchannel), we obtain:

$$p(0) = p_0 + \frac{1}{2}\rho\omega^2\left(R_1^2 - R_0^2\right) \tag{5}$$

This represents the pressure at the upper end (inlet) of the channel ($z = 0$). Integration of the same Eq. 3 along the z-axis within the microchannel from $z = 0$ to a certain position z, coupled with the condition that $p(R_2 - R_1) = p_0$ (i.e., at the channel outlet, the pressure equals the atmospheric pressure), results in:

$$p(z) = p_0 + \frac{1}{2}\rho\omega^2\left[z^2 - \left(\frac{R_1^2 - R_0^2}{L} + L\right)z + \left(R_1^2 - R_0^2\right)\right] \tag{6}$$

where $L = R_2 - R_1$, is the length of the channel. We can see that the pressure variation as a function of position (z) follows a parabolic behavior (z is a second order function). This dependence presents a minimum at:

$$z_V = \frac{1}{2}\left(\frac{R_1^2 - R_0^2}{L} + L\right) \tag{7a}$$

If condition $z_V < L$ is fulfilled, there will be a region in the upper part of the channel (closer to the center of rotation) where the pressure $\Delta p(z) = p(z) - p_0$ is positive, while pressure in the lower part of the channel is negative (Fig. 2b). The former will give rise to "backflow" when the fluid advances from the main radial channel into the T-junction (Fig. 1), whereas the latter will be responsible for a "suction" effect. The magnitude of the suction (i.e., negative pressure) for a certain value R_0 of the liquid in the

reservoir can be obtained by considering $z = z_V$ in Eq. 6 which results in:

$$\Delta p_V = p(z_V) - p_0$$
$$= \frac{1}{2}\rho\omega^2\left[(R_1^2 - R_0^2) - \frac{1}{4}\left(\frac{R_1^2 - R_0^2}{L} + L\right)^2\right] \quad (7b)$$

The maximum value of the negative pressure is manifested just before the reservoir R empties completely ($R_0 = R_1$) and is given by:

$$\Delta p_{V,MAX} = -\frac{1}{8}\rho\omega^2 L^2 \quad (7c)$$

and this maximum value is observed at the midpoint of the main channel.

The separation point between the backflow ($\Delta p > 0$) and suction ($\Delta p < 0$) regions is given by the non-trivial solution of the equation $\Delta p(z) = 0$:

$$z_0 = \frac{R_1^2 - R_0^2}{L} \quad (8)$$

From Eq. 8, the separation point is initially far from the center of rotation: a full reservoir means small values for R_0 (and thus large values for z_0). As the reservoir empties, R_0 gets larger and z_0 gets smaller. At $R_0 = R_1$ (empty reservoir), we get $z_0 = 0$; the separation point is now located at the inlet and the suction region has extended all the way down the main channel (Fig. 2c).

4 Design criteria

In order to find if suction is possible for a given design geometry, the separation point defined by Eq. 8 must fall within the length of the microchannel ($z_0 < L$). Following this condition and using Eq. 8, we have:

$$R_1^2 - R_0^2 < L^2 \quad (9)$$

Taking into account the definition of L,

$$R_2(2R_1 - R_2) < R_0^2 \quad (10)$$

In order to satisfy the conditions imposed by Eq. 10, the term in the parenthesis needs to be positive:

$$2R_1 > R_2 \text{ or } R_1 > \frac{R_2}{2} \quad (11)$$

The criterion shown in (11) is very important for design of a radial channel that can be employed for hydrostatic pumping.

If condition (11) is satisfied, we must know how much liquid is necessary to be present in reservoir R in order to see suction effect (negative pressure) beginning to occur. The critical fluid level $R_{0,c}$ in the reservoir is given by Eq. 10:

$$R_{0,c} = \sqrt{R_2(2R_1 - R_2)} \quad (12)$$

The maximum R_0 is when $R_0 = R_1$ (empty reservoir), and therefore,

$$R_{0,c} < R_0 < R_1 \quad (13)$$

This relationship reveals the range of liquid level in the reservoir that leads to the suction effect.

Both points z_V and z_0 are dependent on the level of the liquid in the reservoir. This means that the point of separation between the backflow and suction regions changes while the reservoir is emptying. From Eq. 8, we see that z_0 gets smaller as R_0 increases: this means that the separation point between the two regimes travels toward the inlet (upward in Fig. 2a). Thus, the suction region becomes larger as the reservoir empties and encompasses the entire channel when the reservoir is completely emptied ($R_0 = R_1 \Rightarrow z_0 = 0$). At this limit, distribution of the pressure along the channel is a symmetric parabola with the minimum in the middle of the channel and $p(z) = p_0$ at both ends (Fig. 2c). Due to the dynamic nature of the separation point z_0, as a rule of thumb one can consider the midpoint of the microchannel as an appropriate position for a junction that corresponds to highest level of negative pressure generated (i.e., z_V when reservoir R is empty).

If we want to calculate the level of fluid in the reservoir that is necessary to start the suction at a certain point within the channel (e.g., a T-junction is placed at z_T), we have to stipulate the condition that the separation point defined by Eq. 8 is located at that point. We impose $z_0 = z_T$

$$z_T = R_T - R_1 = \frac{R_1^2 - R_0^2}{L}$$

and obtain:

$$R_{0,start} = \sqrt{R_1^2 - (R_T - R_1)(R_2 - R_1)} \quad (14)$$

The design criteria presented in this section can be utilized to determine (1) the position of the radial microchannel to create hydrostatic suction on the microfluidic CD (Eq. 11), (2) the level of fluid necessary to be present in the reservoir to start the suction (Eq. 12), and (3) the combination of the two which gives the fluid level in the reservoir necessary to generate suction at a specific point within the microchannel (Eq. 14).

Let us consider the following as an example of design criteria used to fabricate fluidic structures on the CD (Fig. 1-S):

$R_1 = 20.99$ mm,

$R_2 = 34.05$ mm, and

R_T the position of the T-junction $= 28.18$ mm

These parameters fulfill the theoretical conditions for suction generation in a radial microchannel on a rotating
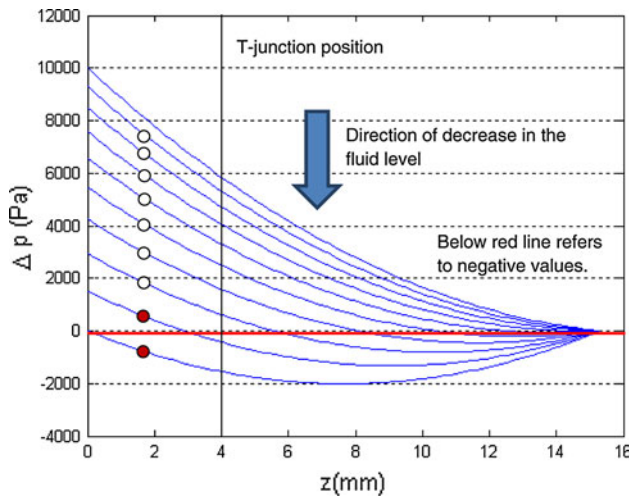
Fig. 3 Evolution of the profile of the static pressure along the microchannel. Different *curves* correspond to different levels of the liquid in the reservoir: *upper curve* is for a full reservoir and *lowest curve* is applicable for a nearly empty reservoir. *Vertical full line* marks the position of the T-junction in experiment. *Filled bullets* mark the curves responsible for suctions at the junction, whereas *empty circles* indicate backflow. The *arrow* indicates direction of evolution of the series of pressure profiles as the reservoir empties

disk. As for the level of fluid at which suction point (z_0) begins to propagate from the outlet toward the inlet, Eq. 12 gives $R_{0,c} = 6.48$ mm. The fluid level in the reservoir at which the suction point arrives at the T-junction is given by Eq. 14 as:

$$R_{0,start} = \sqrt{R_1^2 - (R_T - R_1)(R_2 - R_1)} = 18.62 \text{ mm}$$

This means that the last 2 mm of fluid in the blue reservoir is responsible for generating the highest suction. Figure 3 shows the theoretical pressure profiles within the microchannel for 10 equidistant fluid levels in the reservoir. The bottom two curves (marked with filled red bullets) show suction at the T-junction, and the rest represent backflow into the T-junction (positive pressure).
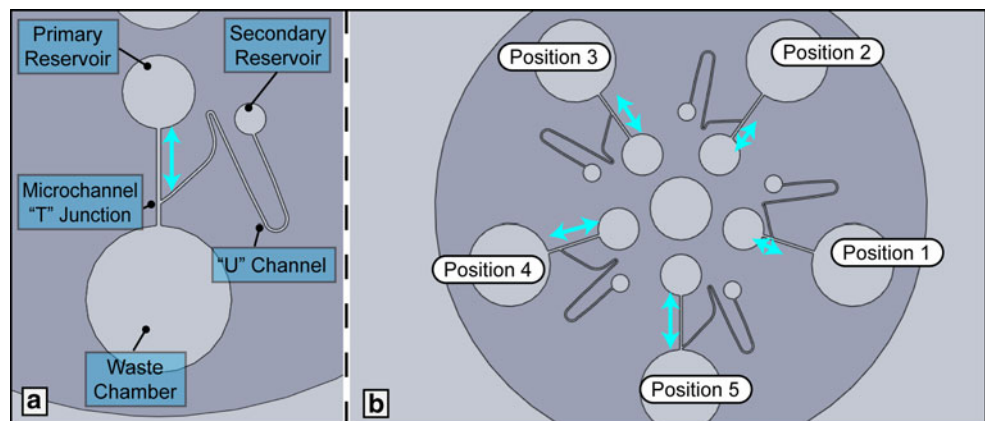
The minimum pressure difference required for priming the siphon is obtained by:

$$\Delta p_{priming} = \frac{1}{2}\rho\omega^2\left(R_{0,red}^2 - R_{crest}^2\right) \quad (15)$$

$R_{0,red}$ and R_{crest} correspond to the level of fluid in the secondary reservoir, and the siphon valve crest, respectively.

5 Experimental

An analysis of the pressures generated along the microchannel inside a spinning disk was necessary to validate the theoretical model. In order to achieve this, a specialized centrifugal microfluidic design was used to quantify the pressures at specific points along the microchannel connecting the loading and waste reservoirs. Specifically, an additional auxiliary channel (ending in a loading chamber) was connected at one end to the main conduit at a T-junction. In the middle of the auxiliary channel, a U-shaped feature was also incorporated. When the U-channel is loaded with liquid, it acts as a "pressure gauge": the differences in height of the liquid traveling in the U-channel could be used to infer pressure changes at the T-junction (Fig. 4a). To reliably test the analytical model, five different designs were arrayed around the disk. The main difference between various designs was the location of the T-junction along the length of the main channel (Fig. 4b).

The designs were incorporated on microfluidic disks manufactured using rapid prototyping techniques. The disk fabrication consists of an assembly of polycarbonate (PC) sheets (1.016 mm thick) and double-sided pressure-sensitive adhesive (PSA) layers (0.1 mm thick). Briefly, a basic microfluidic CD consists of five layers: three PC layers which contain the larger chambers and two thin PSA layers that include the smaller microfluidic channels and allow for sealing of the assembly (main microchannel and U-channel

Fig. 4 Schematics of the experimental disk design. **a** A close-up showing the components of the fluidic design; **b** a view of the complete disk with five designs. The *arrows* highlight the difference in the positions of the T-junctions for various designs

Fig. 5 A series of still images showing the initial, midway, and final time frames for various T-junction positions along the main channel (highlighted by the *double headed blue arrows*). Notice that the hydrostatic head decreases with time as the fluid empties from the main reservoir. **a** shows position 1 (*red arrows* to the left of U-channel denote the initial liquid levels in the microchannel, while the *green arrows* located to the right show final liquid levels in the U-channel) where there is first a positive pressure and thus a decreasing height within U-channel, followed by an equalization where the levels balance out to match centrifugal pressure, and finally a negative pressure resulting in a height change of 0.5 mm. **b–d** show positions 2, 3, and 4, with height changes estimated at 1.0, 1.0, and 0.5 mm, respectively. There was no observable change in the level of fluid during rotation for the design with T-junction in position 5 (not shown)
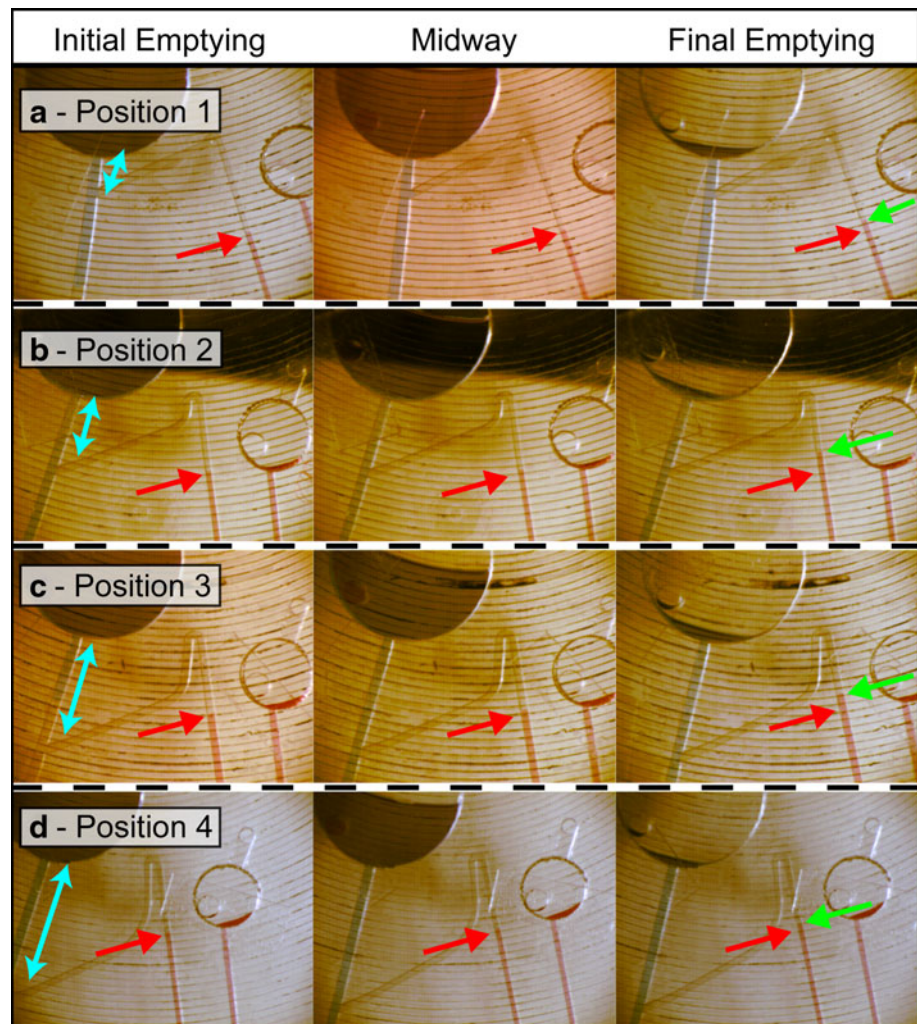
are both made with a 0.1-mm-thick PSA that translates to the height of these microfeatures). PC (McMaster Carr, USA) blanks were cut using a computer numerical controlled (CNC) machine, while the PSA (Flexcon, USA) sheets were cut using a standard cutter-plotter; more details can be found in (Siegrist et al. 2010).

Once fabricated and assembled, microfluidic CDs are mounted on a spin stand, with a vertically positioned digitally controlled brushless servo motor (Pacific Scientific) used to spin the disks. Motor control software allows for controlled acceleration, spin rate, and deceleration of the CDs. In order to visualize the fluids in motion, an optical system is positioned above the motor setup. The arrangement includes a triggering mechanism to allow for selective image collection during rotation: one image is taken per revolution. Image processing software thus enables analysis of particular areas of the disk throughout experimentation. To assist in visualization, an additional stand alone measurement disk was fabricated and mounted below the fluidic CDs. The concentric rings on the disk (0.5 mm

apart) assisted in acquiring accurate meniscus locations during high-speed rotation (as seen in Fig. 5).

6 Results

The experimental results are summarized in Table 1. The table contains records of the meniscus locations for each design. The fluid rise was different for the various designs since suction pressure depends on the position of the T-junction along the main channel. The distance that the fluid traveled in each U-channel was measured by counting the number of divisions on the background concentric circles. The experimental suction pressure generated was calculated from the liquid column rise using Eq. 5.

Position 1 with the T-junction closest to the inlet of the microchannel presented both "backflow" due to positive pressure and "suction" due to negative pressure generation (Fig. 5a). The positive pressure generation was verified by initial fluid level descending in the U-channel. It was then

Table 1 Experimental results include change in the location of the fluid meniscus for various designs

Position	Distance from inlet to T-junction (mm)	Fluid level change in the U-channel (mm)	Distance from T-junction to fluid level in U-channel (mm)	Pressure generated (Pa)	Theoretical pressure (Pa)
p1	2.30	–0.5, 0, +0.5	0.71	–814	–847
p2	4.87	+1.0	1.86	–1611	–1365
p3	7.43	+1.0	4.42	–1611	–1431
p4	9.99	+0.5	6.98	–814	–1048
p5	12.55	0	9.54	0	–215

The fluid level change was measured by using a measurement disk with 0.5-mm-spaced concentric circles. The positions of the T-junction are set by the design and are reported as distances from the channel inlet to the middle of the junction. In the column for fluid level change, plus signs show fluid level rise, "0" indicates no change, and minus sign corresponds to the lowering of fluid level in the capillary

followed by a rise in the fluid level to equilibrium and finally, when fluid almost emptied from the primary reservoir, the red fluid in the U-channel moved further up to confirm a negative pressure change. The backflow effect was only observed for position 1 which was consistent with predictions from the analytical model. From the analytical model, we expect the separation point Z_0 to move toward the inlet of the microchannel as fluid in the primary reservoir empties (Eq. 8). If position of the T-junction is closer to the channel inlet to be in the backflow region of the pressure profile (Fig. 2b), the junction experiences positive pressure until the primary fluid empties and the separation point Z_0 moves above the T-junction position at which point "suction" begins to occur. For all the other four T-junction positions, backflow did not occur, since the

separation point was above the junction even at the initial point, and thus, only negative pressure was experienced at the junction (though not at its maximum level which occurs at the middle of channel when all the primary fluid is emptied). Fluid in the U-bend in position 5 did not experience any significant pressure change during rotation as expected from the theory, and thus, no meniscus movement was observed.

In order to evaluate the experimental pressure profile along the microchannel and compare it to the prediction from the analytical model, we have calculated the theoretical pressure changes using Eq. 6 for the time point at which the primary reservoir is almost emptied. Figure 6 shows that the experimental results are consistent with the analytical model giving a parabolic pressure profile along the microchannel. The experimentally determined pressure values and their corresponding theoretically predicted counterparts for each of the five designs were plotted with the MathWorks software (MatLab), and cubic spline interpolation was used to draw the plots. The error bars on the experimental pressure graph are reflecting the meniscus position uncertainty of ± 125 microns (since the guiding lines on the background disk are 500 microns apart).
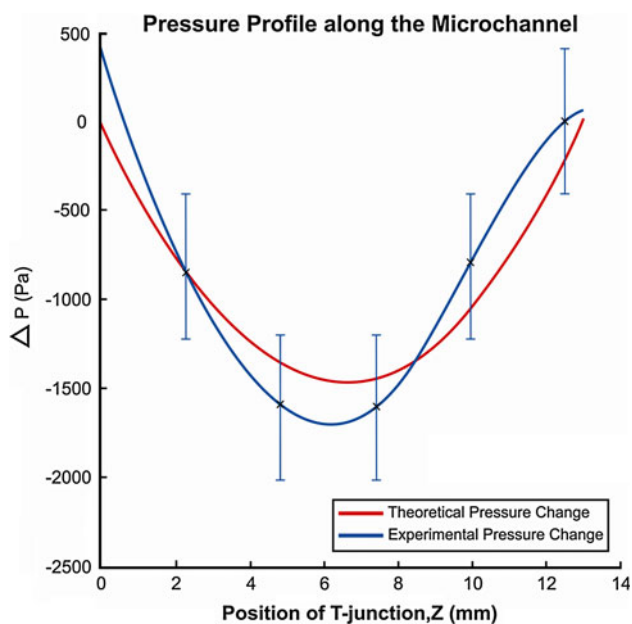
7 Valving applications

The suction-enhanced siphoning technique can be used as a priming mechanism for siphon valves under hydrophobic conditions. Siphoning in CD fluidics utilizes microchannel structures that extend above the radial position of a liquid reservoir to a position radially below that reservoir (Ducrée et al. 2007). Typical operation of a siphon valve corresponds to the interplay between capillary force that is responsible for raising the fluid up the microchannel for priming the siphon valve and centrifugal force that pushes fluid down (radially outwards) and prevents priming. Therefore, when rotation speed is lowered sufficiently, the capillary force can overcome centrifugal force and raise the fluid for priming. After priming, the bulk fluid can move
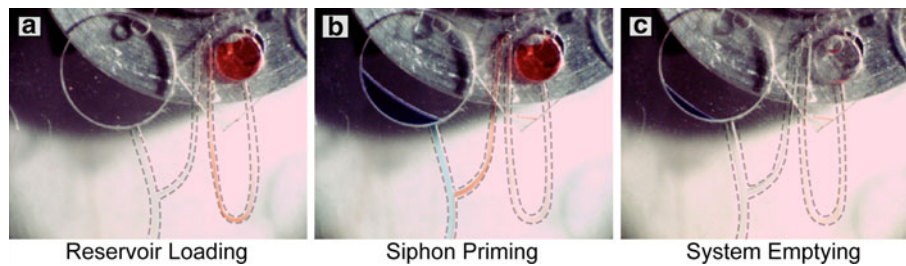

Fig. 6 Experimental versus theoretical pressure profiles in a rotating radial microchannel. The *error bars* represent $\pm$ 0.125 mm uncertainty in measuring the distances that the *red* fluid moved within the U-channel. Measuring circles are spaced in 0.5-mm intervals, and level changes below 0.125 mm were not distinguishable

Fig. 7 a Loading secondary fluid and equalization in the U-channel; **b** loading fluid into the primary reservoir, emptying, and priming of the siphon; **c** continued emptying of the primary reservoir and complete emptying of the secondary reservoir after siphon priming. The microchannels are outlined for clarity

through the conduits downstream by increasing the centrifugal force at higher rotation speeds (Siegrist et al. 2010). As fluids can be held in place until the priming event occurs, siphoning is a common technique to valve fluids in centrifugal microfluidics. It should be emphasized that the described siphoning mechanism would only work in disks made of hydrophilic materials, thus restricting the application of hydrophilic siphoning to a limited set of conditions. The ability of hydrostatic pressure pumps to generate suction in similar structures (i.e., the U-channel pressure gauge shown in the previous sections) led us to design "hydrophobic" siphon valves on disk platforms that could be primed by the suction effect.

The practical role of the hydrostatic pressure pump in priming hydrophobic siphons and emptying secondary reservoirs was validated by carrying out the following experiment; about 20 μl of colored aqueous solution, shown in red, is loaded into the siphon chamber and the CD is spun up to 6,000 RPM to equalize the fluid levels in the U-channel (equilibrium is reached due to centrifugal force and the U-shape geometry as seen in Fig. 7a). The second step is to load about 90 μl of blue dye into the primary reservoir and start spinning at 2,500 RPM (the ramp rate was set at 10,000 RPM/s to reach the constant 2,500 RPM in fraction of a second). The centrifugal force drives the blue dye outward through the microchannel which establishes the transient hydrostatic pressure head as discussed earlier in this report. As the primary chamber continues to empty, the separation point between the backflow and suction regions starts to move upward along the microchannel and ultimately expose the T-junction to a negative pressure. This causes vacuum in the siphon channel which draws the secondary reservoir's fluid (red dye) over the siphon crest and then into the main microchannel (Fig. 7b). At this point, the siphon is "primed" and during continued rotation, the reservoir is emptied (Fig. 7c). It should be noted that, consistent with the analytical predictions, only when the primary reservoir has released approximately 2/3 of its total fluid volume (~ 65 μl in our experiment) was the secondary reservoir's fluid drawn over the restricting crest (the video file is available as a supplementary material).

8 Discussions and conclusion

Conceptualized through analytical modeling and verified through a series of experiments, the suction-enhanced siphon valving represents an original approach to pumping a target fluid short distances toward the CD center by utilizing outward centrifugal flow of a second bulk fluid. By exploiting the pressure differences created when centrifugal flows are established in primary microchannels, the valving mechanism allows for efficient storage and release of auxiliary fluids located in adjacent reservoirs.

In general, this work expands the use of siphons as valving structures for centrifugal microfluidic devices. The hydrophobic siphon valves are advantageous over commonly used siphoning techniques, owning no dependence on specialized hydrophilic materials nor relying on surface treatments needed for capillary pumping (García-Cordero et al. 2010a; Siegrist et al. 2010). Additionally, in comparison with pneumatic pumping (which has also been shown to prime siphons using the relaxation of compressed air for driving the fluids over the siphon crest under hydrophobic conditions), the presented technique requires no specialized air ballast chambers or spin profiles (Gorkin et al. 2010b). Furthermore, the hydrophobic siphon design describes a new category of valving that, while passive in nature, shares some advantages associated with active valving systems.[1] Until recently, most active valving methods required a physical barrier and external activation mechanism to operate, for example, IR laser/halogen lamp actuation of waxes in Park et al. (2007) and Abi-Samra et al. (2011), and laser ablation of thermoplastic barriers demonstrated in García-Cordero et al. (2010b). Instead, the suction-enhanced siphon system uses an internal (as opposed to external) self-contained actuator, solely relying on the pressure gradient generated during centrifugal pumping of a primary fluid to open the valve. Potentially, the method allows for the preloading of multiple chambers on a disk that only release at specific times; these disks can

---

[1] The authors have delineated passive/active techniques by the need for additional actuation besides stop-and-go CD rotation.

be loaded during assembly process, and the only requirement for release is the centrifugal flow of another fluid through a microchannel connected to the siphon via a T-junction.

Overall, the suction-enhanced siphon valving technique can be utilized in complex multi-step chemical and biological processes on a disk. For example, in the development of integrated immunoassays in CD-based designs, suction-enhanced siphoning systems would allow the capability to release consecutive reagents on demand to create antigen/antibody/label complexes. Potentially, as assays typically require a mixing step after valving two liquids, further work could examine the mixing efficiency during valve opening as well. Additional studies can also be performed to model the dynamics of the pressure change in the auxiliary channel and in the auxiliary reservoir. In conclusion, the hydrostatic pressure pump and pressure-activated hydrophobic siphon valve represent additional techniques in the growing "toolbox" of designs developed to overcome the ramifications of unidirectional flow of centrifugal microfluidics. The techniques allow for greater utilization of the surface area on the disk without increasing the complexity and easily adapt to existing manufacturing technologies for polymer-based centrifugal fluidic platforms.

References

Abi-Samra K, Hanson R, Madou M, Gorkin R (2011) Infrared controlled waxes for liquid handling and storage on a CD-microfluidic platform. Lab Chip 11:723–726

Beaulieu I, Geissler M, Mauzeroll J (2009) Oxygen plasma treatment of polystyrene and zeonor: substrates for adhesion of patterned cells. Langmuir 25:7169–7176

Becker H, Gärtner C (2008) Polymer microfabrication technologies for microfluidic systems. Anal Bioanal Chem 390:89–111

Burtis C, Mailen J, Johnson W, Scott C, Tiffany T, Anderson N (1972) Development of a miniature fast analyzer. Clin Chem 18:753–761

Ducrée J, Haeberle S, Lutz S, Pausch S, Stetten F, Zengerle R (2007) The centrifugal microfluidic Bio-Disk platform. J Micromech Microeng 17:S103–S115

García-Cordero J, Basabe-Desmonts L, Ducrée J, Lee L, Ricco A (2010a) Liquid recirculation in microfluidic channels by the interplay of capillary and centrifugal forces. Microfluid Nanofluid 9:695–703

García-Cordero J, Kurzbuch D, Benito-Lopez F, Diamond D, Lee L, Ricco A (2010b) Optically addressable single-use microfluidic valves by laser printer lithography. Lab Chip 10:2680–2687

Gorkin R, Park J, Siegrist J, Amasia M, Lee B, Park J, Kim J, Kim H, Madou M, Cho Y (2010a) Centrifugal microfluidics for biomedical applications. Lab Chip 10:1758–1773

Gorkin R, Liviu C, Madou M, Kido H (2010b) Pneumatic pumping in centrifugal microfluidic platforms. Microfluid Nanofluid 9:541–549

Kido H, Micic M, Smith D, Zoval J, Norton J, Madou M (2007) A novel, compact disc-like centrifugal microfluidics system for cell lysis and sample homogenization. Colloid Surf B 58:44–51

Larsson A, Derand H (2002) Stability of polycarbonate and polystyrene surfaces after hydrophilization with high intensity oxygen RF plasma. J Colloid Interface Sci 246:214–221

Liu M, Zhang J, Liu Y, Lau W, Yang J (2008) Modeling of flow burst flow timing in Lab-on-a-CD systems and its applications in digital chemical analysis. Chem Eng Technol 31:1328–1335

Madou M, Zoval J, Jia G, Kido H, Kim J, Kim N (2006) Lab on a CD. Annu Rev Biomed Eng 8:601–628

Park J, Cho Y, Lee B, Lee J, Ko C (2007) Multifunctional microvalves control by optical illumination on nanoheaters and its application in centrifugal microfluidic devices. Lab Chip 7:557–564

Siegrist J, Gorkin R, Clime L, Roy E, Peytavi R, Kido H, Bergeron M, Veres T, Madou M (2010) Serial siphon valving for centrifugal microfluidic platforms. Microfluid Nanofluid 9:55–63

Steigert J, Brenner T, Grumann M, Riegger L, Lutz S, Zengerle R, Ducrée J (2007) Integrated siphon-based metering and sedimentation of whole blood on a hydrophilic lab-on-a-disk. Biomed Microdevices 9:675–679

Tsao C, DeVoe D (2009) Bonding of thermoplastic polymer microfluidics. Microfluid Nanofluid 6:1–16